Geological Magazine

www.cambridge.org/geo

Petrogenesis and tectonic significance of Kawardha lamproite dykes from the Western Bastar Craton, central India

Tanveer Haidar[1,2], M.P. Manu Prasanth[3], K.R. Hari[4] and Neeraj Vishwakarma[1]

[1]National Institute of Technology, Raipur, Chhattisgarh, India; [2]Geological Survey of India Training Institute, Hyderabad, India; [3]Hubei Key Laboratory of Petroleum Geochemistry and Environment, College of Resources and Environment, Yangtze University, Wuhan, China and [4]Pt. Ravishankar Shukla University, Raipur, Chhattisgarh, India

Original Article

Cite this article: Haidar T, Manu Prasanth MP, Hari KR, and Vishwakarma N. Petrogenesis and tectonic significance of Kawardha lamproite dykes from the Western Bastar Craton, central India. *Geological Magazine* **162**(e30): 1–15. https://doi.org/10.1017/S0016756825100186

Received: 19 March 2024
Revised: 3 April 2025
Accepted: 24 July 2025

Keywords:
Lamproites; petrogenesis; asthenosphere; mantle-metasomatism; Bastar craton

Corresponding author:
M.P. Manu Prasanth;
Email: manu@earth.sinica.edu.tw

Abstract

We present the mineralogy and whole rock geochemistry of the lamproites dykes from the Kawardha area of the Western Bastar Craton. These dykes are characterized by phenocrysts and microphenocrysts of olivine, phlogopite, ulvo-spinel, Cr-spinel and magnetite within the chlorite and carbonate-rich groundmass with rutile and apatite as accessory phases. Mineral chemistry indicates that the lamproites in Kawardha are similar to olivine-phlogopite lamproites and are geochemically similar to other lamproites in the eastern Bastar craton. The Kawardha lamproites are characterized by higher concentrations of MgO (12–20.29 wt%), V (193–502 ppm), Ni (206–823 ppm), Cr (146–1130 ppm), Nb (101–260 ppm), Zr (301–635 ppm), Hf (6–13 ppm) and LREEs. Positive Nb-Ta anomalies and Th, Hf and Zr variations are comparable to other intra-cratonic rift-related lamproites. The geochemical variations (such as REE, HFSE and LILE) are consistent with an asthenospheric mantle source similar to the other lamproites in Bastar craton. Trace element modelling implies a low-degree partial melting (0.1–2%) of phlogopite-bearing garnet-lherzolite and/or phlogopite-bearing spinel-lherzolite mantle source. The widespread Proterozoic rifting events in the Bastar craton likely led to the melting and upwelling of the asthenospheric mantle and which further interacted with the metasomatized lithospheric mantle to form the parental melts of the lamproite dykes of the Kawardha area.

1. Introduction

Lamproites are rare, hydrous, mafic-ultramafic (Mg# = Mg/Mg+Fe > 60%) to ultrapotassic (K/Na > 3) and peralkaline ($Na_2O + K_2O > Al_2O_3$) igneous rocks, and are characterized by their exceptional enrichment of compatible and incompatible trace elements (Bergman, 1987; Foley *et al.* 1987; Kjarsgaard *et al.* 2009). The lamproites are often derived from the deepest mantle sources, and their unique geochemistry and distinct modes of origin are often utilized to study large-scale geodynamic processes and deep volatile fluxes (Thompson *et al.* 1990; Gibson *et al.* 1995; Martinotti *et al.* 2006; Prelević *et al.* 2010; Huang *et al.* 2010; Yilmaz, 2010; Rukhlov, Blinova & Pawlowicz, 2013; Liu *et al.* 2014; Stern, Leybourne & Tsujimori, 2016).

In general, lamproite magmas are derived from the partial melting of heterogeneous mantle sources that include geochemically enriched domains (metasomatized) of the subcontinental lithospheric mantle (Foley, 1992; Murphy, Collerson & Kamber, 2002; Davies *et al.* 2006), and melts from sub-lithospheric sources further interacts with metasomatized subcontinental lithospheric domains during the melt transit to the surface (Sarkar *et al.* 2022). However, the origin of lamproites and the enrichment of incompatible trace elements are debated. Several models for their origin have been proposed, which include (1) ancient subducted continental material in the mantle transition zone (Murphy, Collerson & Kamber, 2002; Rapp *et al.* 2008), (2) recycled crustal materials in subcontinental lithospheric mantle (SCLM) (Avanzinelli *et al.* 2009; Prelević *et al.* 2010; Tommasini, Avanzinelli & Conticelli, 2011), (3) enrichment of a previously depleted SCLM by metasomatic melts originating either from the asthenosphere or subducted crustal slab (McKenzie, 1989; Foley, 1992; Nelson, 1992; Tainton & McKenzie, 1994; Turner *et al.* 1999; Davies *et al.* 2006; Tappe *et al.* 2008) and (4) direct formation from a heterogeneous mantle plume (Mirnejad & Bell, 2006; Rukhlov, Blinova & Pawlowicz, 2013; Sushchevskaya *et al.* 2014; Santosh *et al.* 2018). Experimental evidence suggests that the primary melts of Si-rich ultrapotassic rocks require high-degree melting of a phlogopite-bearing mantle source. However, Si-deficient ultrapotassic primary melts may originate in the wehrlitic mantle, facilitated by metasomatic phases that are fluxed by volatiles such as H_2O and CO_2 (Gülmez *et al.* 2023; Förster *et al.* 2019a; Wang, Foley & Prelevic, 2017). Förster *et al.* (2019b) investigated the effects of mantle metasomatism through sediment and hydrous mantle melts using a two-layer reaction experiment. The results show that sediment-dunite interactions at low

temperatures (<1000°C) form K-enriched phlogopite-pyroxenite, while higher temperature reactions (1200°C) with hydrous basanite led to enrichment in K and K/Na and the generation of lamproite melt. It has also been demonstrated that experimental partial melts of K-richterite-bearing mica pyroxenites produce melts similar to lamproites (Ezad & Foley, 2022).

The emplacement of lamproites in central India has been correlated with the Paleoproterozoic plume-induced global rifting events (Santosh *et al.* 2018). The central Indian craton, also known as the Bastar craton, records evidence of distinct lamproite magmatism in the eastern and western domains. The Eastern Bastar Craton (EBC), records lamproite magmatism at Kalmidadar, Amlidadar, Darlimunda, Parkom, Sakri (Sahu *et al.* 2013; Chalapathi Rao *et al.* 2015; Santosh *et al.* 2018) and Khadka (Yellappa, Chalapathi Rao & Chetty, 2010). However, from the Western Bastar Craton (WBC), only Kawardha lamproites (Lakra & Kujur, 2021) have been reported so far. The lamproite magmatism in the EBC is correlated with the widespread 1.1 Ga extensional magmatic flux associated with the Rodinia supercontinent. The EBC lamproites are formed from a metasomatized subcontinental lithospheric mantle source interacting with the upwelling asthenosphere melt (Sahu *et al.* 2013; Chalapathi Rao *et al.* 2015; Santosh *et al.* 2018). Similarly, the Kawardha lamproites in WBC are proposed to be derived from the metasomatized SCLM sources. The source of carbonate-rich fluids/melts has been attributed to the subduction recycling of the Archean continental lithosphere (Lakra & Kujur, 2021). However, the petrogenetic mechanisms and the tectonic context of lamproite magmatism in the WBC still need to be explored further. Moreover, the detailed geochemical and petrological studies of this rare lamproite occurrence in the Kawardha area of WBC are also significant to understanding the crust-mantle processes in the WBC. In the present study, we used whole-rock geochemistry and mineral chemical analysis to investigate the petrogenetic and tectonic aspects of Kawardha lamproites from WBC. We also evaluated the geochemistry of previously reported lamproites from EBC to delineate regional variations in the source mantle characteristics of lamproite magma generation in Bastar craton and their emplacement mechanisms.

2. Geological framework and study area

The Bastar craton is situated in the central part of the Indian shield (Fig. 1) (Meert *et al.* 2010). Geographically, the north-eastern periphery of the Bastar craton is bordered by the Mahanadi lineament, which separates it from the Singhbhum craton, while the south-western boundary of the craton is marked by the Godavari lineament, which separates it from Dharwar craton. The southeastern and northern margins of the craton are outlined by the Eastern Ghat Mobile Belt and Central Indian Tectonic Zone, respectively. The craton encompasses crustal components from Mesoarchean to Neoproterozoic (Santosh *et al.* 2020; Manu Prasanth *et al.* 2023). This craton is subdivided into two distinct blocks: WBC and EBC, and their boundary is marked by the Kotri-Dongargarh orogeny, also known as Central Bastar Orogen (Santosh *et al.* 2020).

The Bastar craton consists of five major tectonic belts spanning from Archean to Proterozoic, which are Sausar-Chilpi belt (Mishra & Mohanty, 2021), Bengpal-Sukma belt (Ghosh, 2004), Sonakhan greenstone belt (Deshmukh *et al.* 2018; Manu Prasanth *et al.* 2018, 2019), Amgaon belt (Rajesh *et al.* 2009) and Kotri-Dongargarh belt (Manu Prasanth *et al.* 2023). The craton also encompasses three supracrustal sequences: Dongargarh, Sakoli and Sausar suites (Mohanty, 2015; Santosh *et al.* 2018). Among these, the Bengpal and Sukma groups are the oldest granitic rocks in the craton, with the ages of ca. 3561 Ma (Ghosh, 2004) and ca. 3582 Ma (Rajesh *et al.* 2009). The Chilpi rock group represents the youngest rock formations of age 1850–2050 Ma (Mohanty, 2021). Paleoarchean (3.5–3.7 Ga) tonalite trondhjemite gneisses (TTGs) represent the basement ages of the craton (Ghosh, 2004). The U Pb zircon ages of the TTGs range from 3561 ± 11 Ma (Ghosh, 2004), 3583 ± 4 Ma (Rajesh *et al.* 2009) to 3726 ± 22 Ma (Ratre *et al.* 2010). Paleoproterozoic to Mesoproterozoic lamproite magmatism (Yellappa, Chalapathi Rao & Chetty, 2010; Sahu *et al.* 2013; Chalapathi Rao *et al.* 2015; Santosh *et al.* 2018) has been reported

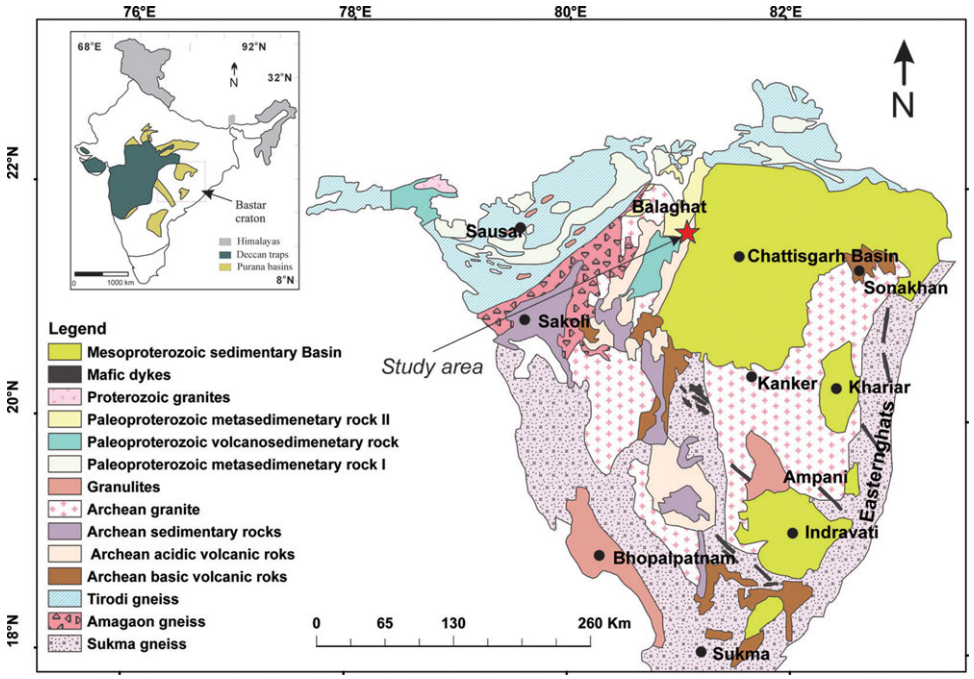

Figure 1. Generalized geological map of the Bastar craton showing the location of Kawardha Lamproites. The inset map illustrates the generalized geology of the Indian subcontinent and the location of the Bastar craton (Modified after Meert *et al.* 2010).

https://doi.org/10.1017/S0016756825100186 Published online by Cambridge University Press

from Darlimunda (2473 ± 8 Ga, Santosh *et al.* 2018), Khadka (1.88 Ga, Yellappa, Chalapathi Rao & Chetty, 2010), Sakri (1045 ± 9 Ma, Chalapathi Rao *et al.* 2015) and Nuapada (1055 ± 10 Ma, Sahu *et al.* 2013) areas. Lamproites of the craton are correlated with two distinct magmatic events. The oldest Nuapada lamproites are correlated with the 2.2 Ga rifting event and a Paleoproterozoic large igneous province event (Santosh *et al.* 2018). Other lamproites represent the late Mesoproterozoic magma flux, where it has been correlated with the rifting events associated with the Rodinia supercontinent (Chalapathi Rao *et al.* 2015).

The study area, located in the north-western fringe of the Chhattisgarh basin within the Bastar craton (Fig. 1), comprises the Chilpi group, volcanics of the Nandgaon group and the basaltic lava flows of the Deccan Traps (Lakra & Kujur, 2021). The Chilpi group forms a linear north-south trending belt, extending approximately 100 km, and consists predominantly of low-grade metasedimentary sequences (Mishra & Mohanty, 2021). It represents the youngest rock unit in the region, with an estimated age range of 1850–2050 Ma (Mohanty, 2021). The Pitepani andesites and Bijli rhyolites of the Nandgaon group are the oldest litho-units (~2663 Ma; Manikyamba *et al.* 2016). The entire sequence is further overlain by Chhattisgarh Supergroup.

The Kawardha Lamproites intrude on the Paleoproterozoic meta-andesites of the Nandgaon group (Figs. 2, 3). Two clusters of lamproite occurrences can be noticed in the Piparadhar and Maharajpur areas of the Kawardha district (Fig. 2, insets a and b) (Lakra & Kujur, 2021). The studied lamproites dykes are small in dimension (10–40 m length) and occur as isolated exposures within the meta-andesites (Fig. 3). More than ten dykes have been identified as lamproites, of which three are located in the Piparadhar area, and more than seven are confined in the Maharajpur area. The general trend of the studied lamproite dykes is NW-SE. Numerous secondary quartz and carbonate veins traversing the exposed lamproite dykes indicate possible post-

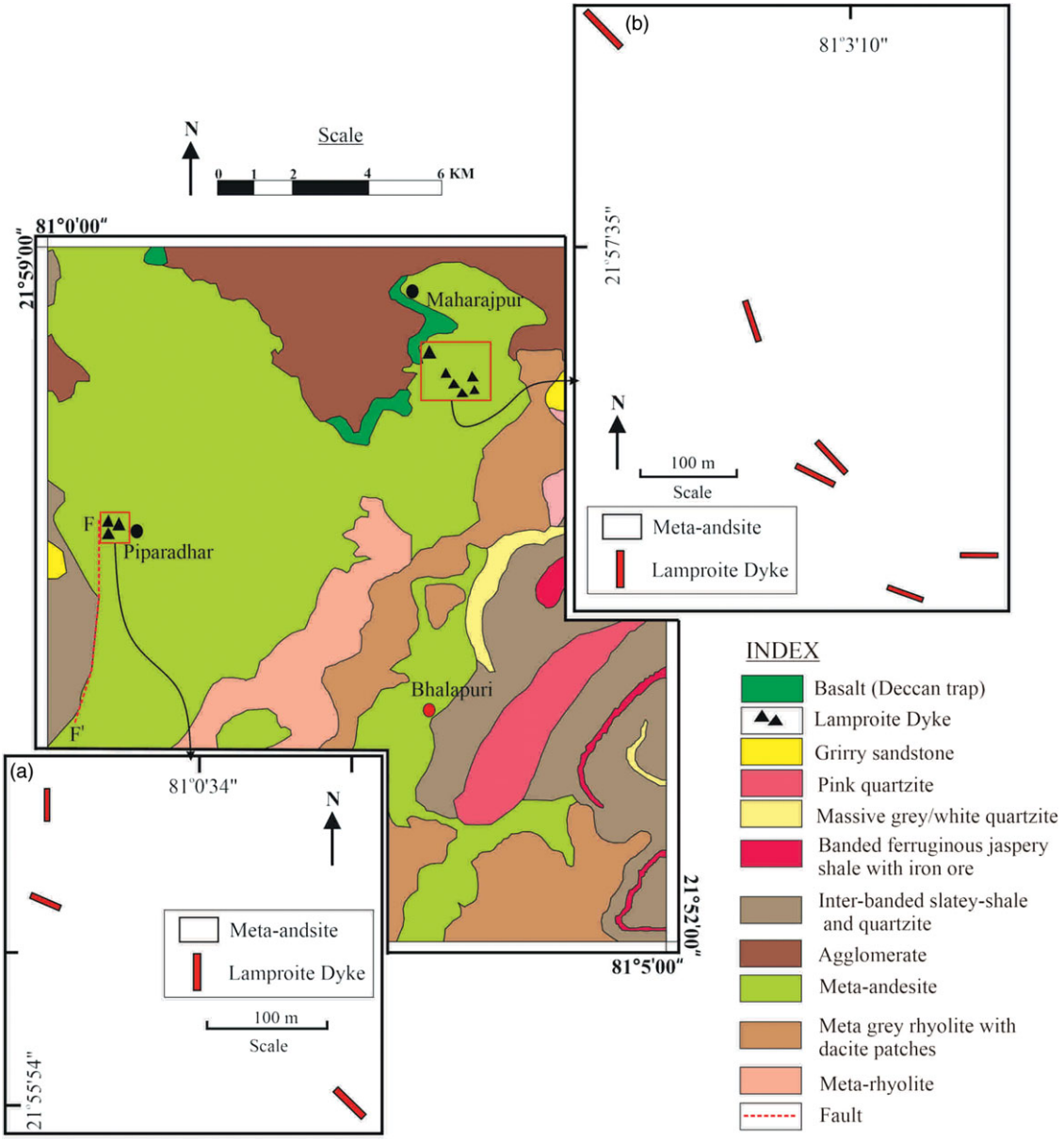

Figure 2. Generalized geological map of the Kawardha lamproite with the study area indicated within the boxes (modified after Lakra & Kujur, 2021). The insets a (Piparadhar cluster) & b (Maharajpur cluster) show the location and trend of the studied lamproite dykes.

https://doi.org/10.1017/S0016756825100186 Published online by Cambridge University Press

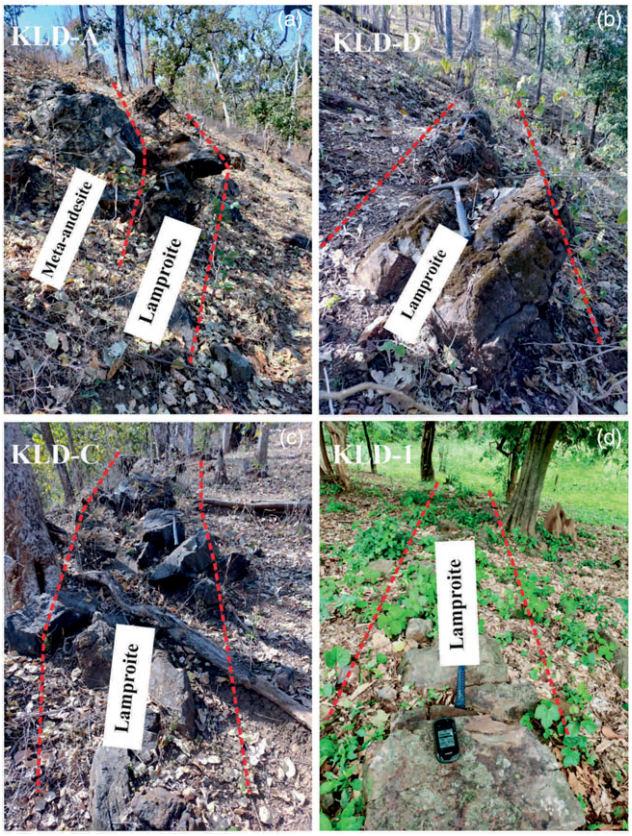

Figure 3. Representative field photographs (a, b, c & d) of Kawardha lamproite showing the studied lamproite dykes intruded within the meta-andesite of the Nandgaon group and occur as isolated bodies. The length of the hammer is 13 inches, and the width of the hammerhead is 6.4 inches.

magmatic alteration. Field details, which include the trend, dimensions, coordinates and key field observations, are given in Supplementary Table S1.

3. Sample preparation and analytical techniques

Whole-rock major and trace element geochemistry of eighteen representative samples were analyzed at the Geochemistry Division, Council of Scientific and Industrial Research-National Geophysical Research Institute (CSIR-NGRI), Hyderabad. *X-ray fluorescence* (XRF) spectrometer (Phillips MagiX PRO Model 2440) was used for the major element analysis. The pressed pellets of the rock powders were used for the analysis. The details of the analytical methodology, including data gathering, accuracy, detection limits and equipment calibration, are given in Krishna, Khanna & Mohan (2016). The trace and rare earth element concentrations were measured using a High-Resolution-Inductively Coupled Plasma Mass Spectrometer (HR-ICP-MS). The techniques used in sample digestion, instrumentation parameters and data acquisition are in Satyanarayanan *et al.* (2018). The representative major and trace element geochemistry data are presented in Supplementary Table S2. MY-4 (IGEM, Russia) and SARM-39 (MINTEK, RSA) are the internal standards for major oxides and trace element analysis, respectively.

Mineral chemistry and back-scattered electron images of selected silicate and opaque minerals of lamproite dykes were analyzed using CAMECA SX Five electron microprobe analyzer (EPMA) with *five wavelength-dispersive* spectrometers at EPMA laboratory of Indian Institute of Technology (IIT), Bombay. The 15 keV accelerating voltage and a 20 nA beam current were used by the operating EPMA source. The equipment has a 1µm beam size, and analysis has a dwell period of around three minutes for each point. The representative mineral chemistry data are presented in Supplementary Tables (S3, S4 & S5). The internal standards, precision, accuracy and detection limits of the employed geochemical analysis are provided in Supplementary Table S8.

4. Results

4.a. Petrography and mineral chemistry

The Kawardha lamproites exhibit signs of extensive alteration; however, primary textural features of the major minerals are well-preserved. Olivine phenocrysts are completely pseudomorphosed by calcite and chlorites, potentially indicating secondary alteration processes such as chloritization and carbonatization. Representative photomicrographs of Kawardha lamproite are presented in Fig. 4, showcasing phenocrysts and microphenocrysts of pseudomorphic olivine, phlogopite and spinel set within a chlorite and carbonate-rich groundmass. Overall, a porphyritic texture can be observed with olivine (pseudomorph) as a phenocrystic phase (Fig. 4a). Some of the important petrographic observations of samples from each lamproite dyke have been provided in Table 1.

Phenocrysts of phlogopite exhibit straw-yellow with a reddish undertone, which is commonly observed in Ti-rich micas (Fig. 4b) (Mitchell & Bergman, 1991; see also Supplementary Table S3). These grains display extinction parallel to cleavages (Fig. 4c) and exhibit compositional gradients from the core to the rim (Fig. 4d), as well as localized signs of chlorite alteration. The groundmass is rich in carbonate and chlorite, and it may be secondary. It also contains rutile, acicular apatite and euhedral grains of spinel (Fig. 4e, f). The mineral compositions of selected mineral grains are presented in Supplementary Tables S3, S4 and S5, and their geochemical variation has been discussed as follows:

4.a.1. Phlogopite

The Mg# (Mg/Mg + Fe^{+2} > 65%; Fig. 6a) suggests that phlogopite is a prominent mica phase. The compositional variation of TiO_2 and Al_2O_3 in phlogopites ranges from 1.59 to 5.27 wt% and 9.86 to 13.48%, respectively (Supplementary Table S3). The TiO_2 and Al_2O_3 concentrations of phlogopite are falling close to lamproite field rather than alnoite or minette (Fig. 5). Due to their (Si + Al) composition being less than 8 pfu (Fig. 6b), all of the phlogopites have a considerable amount of tetra-ferric component. Furthermore, octahedral site deficiency and Ti contents of the phlogopite (Fig. 6c) suggest that two significant Ti-accommodating substitution processes were involved, which is also noticeable in micas from the Nuapada lamproite field (Sahu *et al.* 2013). When compared to other lamproites from the EBC, micas in the Kawardha lamproites have much lower TiO_2 values but show a similar range of Al_2O_3 concentrations (Fig. 6d).

4.a.2. Spinel

The composition of spinels in Kawardha lamproites shows an identical ulvo-spinel trend (Fig. 7a), which is analogous to the spinel trend (T2) of lamproites and orangeites (Mitchell, 1995). The Ti, Cr and Fe_T concentrations (see Supplementary Table S4) suggest three different compositions for the spinel grains, which can be grouped as ulvo-spinel (high Ti and high Fe), chrome-spinel (Cr and high Fe)

https://doi.org/10.1017/S0016756825100186 Published online by Cambridge University Press

Table 1. Summary of salient petrographic features of Kawardha lamproite samples

Dyke	Sample code	Essential mineral phase(s)	Accessory mineral phase(s)	Key observations
Piparadhar Cluster				
KLD-1	1/3, 1/7	Phl	Sp, Rt, Ap, Chl, Qtz	Extensively chloritized Phl
KLD-2*	2/6, 2/7	Phl	Sp, Ap, Chl, Qtz	Complete chloritization of Phl, microscopic veins of Qtz.
KLD-3*	3/5, 3/8	Phl	Sp, Ap, Chl, Qtz	Complete chloritization of Phl, microscopic veins of Qtz.
Maharajpur Cluster				
KLD-A	A1, A2, A3	Ol, Phl	Sp, Ap, C, Chl	Complete pseudomorphed Ol by C, mostly fresh Phl
KLD-B	B1, B2, B3	Ol, Phl	Sp, Rt, Ap, C, Chl, Qtz	Complete pseudomorphed Ol by C and Qtz. Extensively chloritized Phl
KLD-C	C1, C2, C3	Ol, Phl	Sp, Rt, Ap, Il, C, Chl	Complete pseudomorphed Ol by C, mostly fresh Phl
KLD-D	D1, D2, D3	Phl	Sp, Ap, Rt, C, Chl, Qtz	Partial Chloritization of Phl.
KLD-F	F1, F2, F3	Ol, Phl	Sp, Ap, Rt, C, Chl	Complete pseudomorphed Ol by C, complete chloritization of Phl.
KLD-G	G1	Phl	Sp, Ap, C, Chl	Complete chloritization of Phl.

Mineral abbreviations: Ol olivine; Phl phlogopite; Sp spinel; Ap apatite; Rt rutile; Il ilmenite; C carbonates; Chl chlorite; Qtz quartz.
*Extremely altered lamproite dykes.

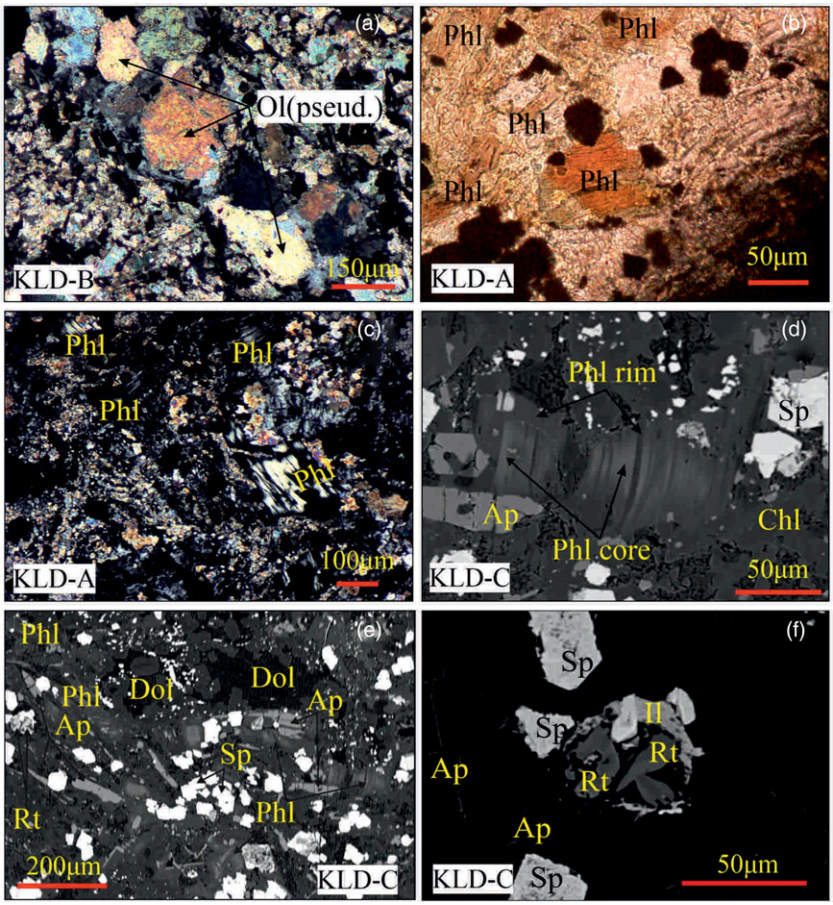

Figure 4. Representative photomicrographs of Kawardha lamproite, (a) showing the pseudomorphic olivine, (b) phlogopites under plain-polarized-light (PPL), (c) in crossed-nicols (XN), (d) backscattered electron (*BSE*) photomicrograph of phlogopite grain with TiO_2 values of core and rim and (e and f) the BSE images of representative mineral grains of phlogopite, spinel, rutile, apatite, chlorite and carbonate. Ol (Pseud.): pseudomorphic olivine, Phl: phlogopites, Sp: spinel, Rt: rutile, Ap: apatite, Dol: dolomite, Chl: chlorite.

and magnetite (high Fe and low Cr-Ti). Concentrations of Mg and Cr in the chrome-spinel (Fig. 7b) suggest that the Kawardha lamproites are non-diamondiferous. $Fe^{+2}/(Fe^{+2}+Mg)$ ratio for the spinel is nearly equal to 1, which is substantially similar to Sakri lamproites (Chalapathi Rao *et al.* 2015). Whereas, Ti /(Ti+Cr+Al) ratio is highest for ulvo-spinel (> 0.85), moderate for chrome-spinel (0.2–0.6) and lowest for magnetite (nearly zero).

4.a.3. Apatite

CaO content in apatites from Kawardha lamproite ranges from 53.23 wt% to 56.57wt%, and P2O5 is up to 40.83 wt%. Apatites are enriched in fluorine (up to 3.68 wt%; supplementary Table S5b) and are classified as fluorapatites. These fluorine-rich apatites are commonly observed in lamproites and/or lamprophyres (Edgar & Charbonneau, 1991; Mitchell & Bergman, 1991; Edgar, Pizzolato &

https://doi.org/10.1017/S0016756825100186 Published online by Cambridge University Press

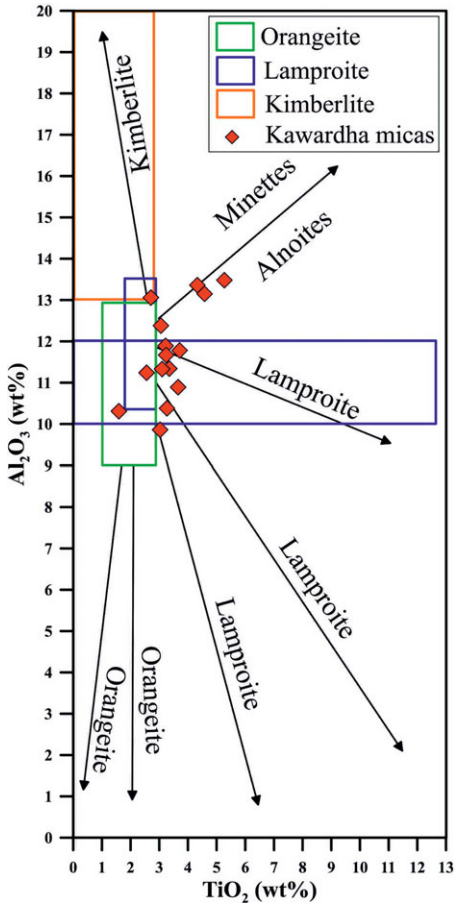

Figure 5. TiO_2 (wt%) vs. Al_2O_3 (wt%) plot showing the compositional variation of phlogopite in the studied Kawardha lamproite. Compositional fields and trends for micas from kimberlite, lamproite, orangeite and minette are taken from Mitchell & Bergman (1991).

Sheen, 1996). The concentration of total FeO (0.1–1.17 wt%), MgO (0–0.9 wt%) and Na2O (0.04–0.4 wt%) is low, possibly suggesting the enrichment of incompatible trace elements like Sr, La and Ce (see Talukdar *et al.* 2018).

4.a.4. Carbonate

Carbonate is not an essential mineral phase in lamproites (Mitchell & Bergman, 1991), but is sometimes present as accessory phases (Chalapathi Rao *et al.* 2010). Our samples show calcite, ankerite and dolomite phases in the groundmass. CaO contents in calcites are high (up to 58.6 wt%) and contain negligible FeO, MgO and MnO. Whereas other carbonate phases are characterized by their high concentrations of FeO, MgO and MnO, which range from 4.14 to 8.4 wt%, 12.62 to 17.8 wt% and 0.3 to 0.95 wt%, respectively (see supplementary Table S5d).

4.a.5. Other groundmass phases

The rutile is mainly iron-bearing and contains FeO up to 1.28 wt%. The chlorites are dominantly pycno-chlorite (Si = 5.4–6.4 apfu) and subsidiary diabantite (Si > 6.4 apfu) in composition.

4.b. Whole-rock major element geochemistry

The bulk rock geochemistry of Kawardha lamproites is presented in Supplementary Table S2. Kawardha lamproites are silica undersaturated (SiO_2 = 22.14–39.91 wt%) with MgO ranging from 12.46 to 20.29 wt%. Their Mg# value (34–50%) suggests an evolved nature, while concertation of other major oxides is highly variable such as Fe_2O_3 (10.6–25.12 wt%), CaO (1.74–22.75 wt%), TiO_2 (3.8–7.48 wt%), P_2O_5 (0.99–3.9 wt%), Al_2O_3 (2.42–5.64 wt%) and loss on ignition (LOI = 2–17.1 wt%). The K_2O concentration in rock samples is very low (<0.71 wt%), which is ascribed to post-magmatic hydrothermal alteration processes (Sahu *et al.* 2013; Santosh *et al.* 2018). Low K_2O content of the samples can also be attributed to chloritization of phlogopites, which is perceptible in the petrography.

4.c. Whole-rock trace element geochemistry

Kawardha lamproites are enriched in rare earth elements (REE = 406–1596 ppm), compatible trace elements such as Ni (206–824 ppm), Cr (160–1184 ppm) and V (215–503 ppm), and incompatible trace elements like Zr (296–635 ppm), Hf (6–13 ppm), Nb (113–260 ppm) and Ta (5.5–17 ppm). In the chondrite normalized diagram (Fig. 8a), Kawardha lamproites exhibit enrichment in lighter rare earth elements (LREE) relative to heavier rare earth elements (HREE) with $(La/Yb)_N$, and value ranges between 50 and 159. However, it is noticeably depleted in several incompatible trace elements with negative anomalies at Rb, K, Ba, Pb, Sr and Zr in the primitive mantle diagram (Fig. 8b). The negative anomalies may have been somewhat influenced by the fluid-mobile behaviour of some of these elements, especially Rb, K, Ba and Pb (e.g., Mirnejad & Bell, 2006; Davies *et al.* 2006; Tappe *et al.* 2008).

5. Discussion

5.a. Lamproitic nature of Kawardha dykes

Potassic minerals such as K-feldspar, and/or kalsilite are not preserved in the Kawardha lamproites, resulting in low K nature, which is similar to other lamproite occurrences of Bastar craton (Sahu *et al.* 2013; Chalapathi Rao *et al.* 2015; Santosh *et al.* 2018). However, the presence of pseudomorphic olivine, Ti-rich phlogopite, ulvo-spinel and fluor-apatite with minor ilmenite and rutile indicates their lamproite affinity. Presence of fluor-apatite (F > 3 wt %) in Kawardha dykes is similar to other lamproite occurrences worldwide (see Jaques, Lewis & Smith, 1986; Edgar and Charbonneau, 1991) and also suggests alkaline nature of the parental melt (Wagner and Velde, 1986; Matchan *et al.* 2009). The alumina content in mica from our samples provides further evidence of their lamproite affinity, with an average Al_2O_3 of 11.74 wt%. This value aligns more closely with the global range of lamproites (5–12 wt%) than lamprophyres, which typically exceed 13 wt% (Rock, 1991). Different geochemical characteristics, including mica compositional trends, spinel trends and the enrichment of incompatible and compatible trace elements, especially high levels of LREEs (up to 1534 ppm) and TiO_2 (up to 6.94 wt%), clearly indicate the lamproitic nature of Kawardha dykes.

5.b. Alteration and crustal contamination

Crustal contamination is a salient process in the modification of the melt chemistry, and it can be estimated by using isotopic and trace element-based geochemical proxies (DePaolo, 1981; Thompson *et al.* 1982; Dostal & Dupuy, 1984). The incompatible trace element ratios such as Ce/Pb and Nb/U are important parameters to access the crustal contamination of the mantle-derived mafic-magmas (Xu, Xu & Zeng, 2017). The Ce/Pb and Nb/U ratios of the mid-oceanic ridge basalts and oceanic island basalts (Ce/Pb = 25 ± 5 and Nb/U = 47 ± 10; Hofmann *et al.* 1986) are

https://doi.org/10.1017/S0016756825100186 Published online by Cambridge University Press

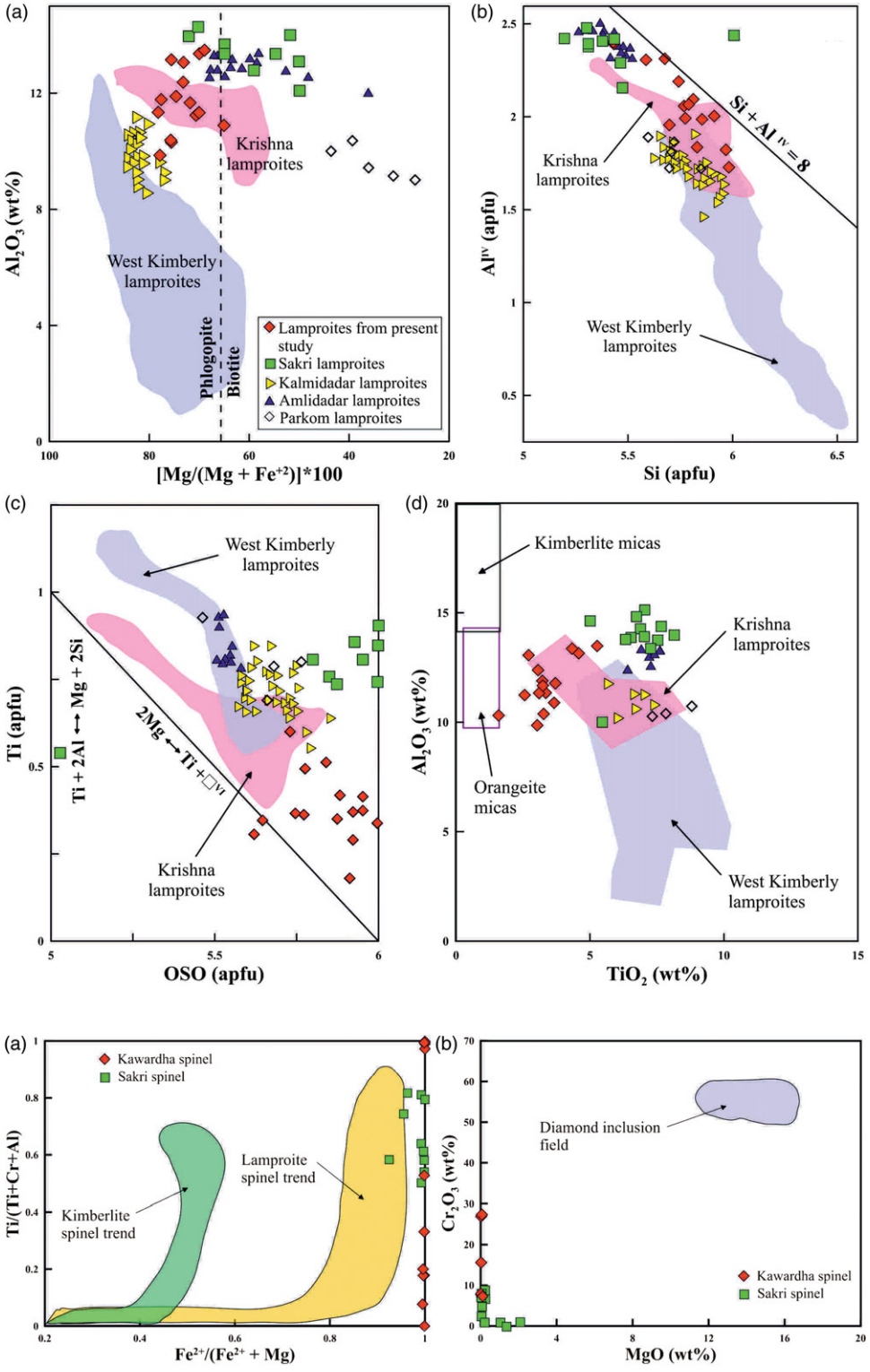

Figure 6. Compositional variation of micas in Kawardha lamproites and other lamproites from Bastar craton (Sahu *et al.* 2013; Chalapathi Rao *et al.* 2015; Santosh *et al.* 2018) compared with that in Krishna lamproites, southern India (Reddy *et al.* 2003; Chalapathi Rao *et al.* 2010) and West Kimberly lamproites (Jaques, Lewis & Smith, 1986; Mitchell & Bergman 1991). (a) Al_2O_3 vs. 100*Mg/(Mg + Fe^{+2}) plot; (b) Tetrahedral Al vs. Si plot; (c) Ti vs. octahedral site occupancy (OSO) plot and (d) TiO_2 vs. Al_2O_3.

Figure 7. Composition of spinel from the Kawardha lamproites projected onto the front face of the (a) oxidized spinel prisms. Compositional variations of spinels from kimberlite and worldwide lamproites are also shown (adapted from Mitchell & Bergman 1991). (b) MgO vs. Cr_2O_3 plot for studied Cr-spinel, with diamond inclusion field after Fipke, Gurney & Moore (1995). The composition of spinel from Sakri lamproites, Bastar craton, is taken from Chalapathi Rao *et al.* (2015).

significantly higher than the continental crust (average Ce/Pb = 3.9 and Nb/U = 6.2; Rudnick & Gao, 2003). The average Ce/Pb and Nb/U ratios of the Kawardha lamproites (46.9 and 61.08, respectively) indicate no significant effect of crustal contamination. In general, crustally contaminated magmas exhibit negative Nb and positive La-Th spikes on the primitive mantle normalized diagrams. Significant enrichments in Rb, Th, K and LREE values (Thompson *et al.* 1982) can also be observed. The Kawardha lamproite exhibits positive anomalies at Nb-Ta-Ti in the primitive mantle normalized diagram (Fig. 8b), contrary to the lavas that have experienced crustal contamination (Nelson, 1992; Murphy, Collerson & Kamber, 2002). Highly fractionated REE pattern on chondrite normalized diagram (Fig. 8a) depleted HREE and Y with the absence of positive anomaly at Eu and Pb, which also precludes the significant crustal contamination (see Nelson, 1992; Murphy, Collerson & Kamber, 2002; Davies *et al.* 2006; Mirnejad & Bell 2006).

https://doi.org/10.1017/S0016756825100186 Published online by Cambridge University Press

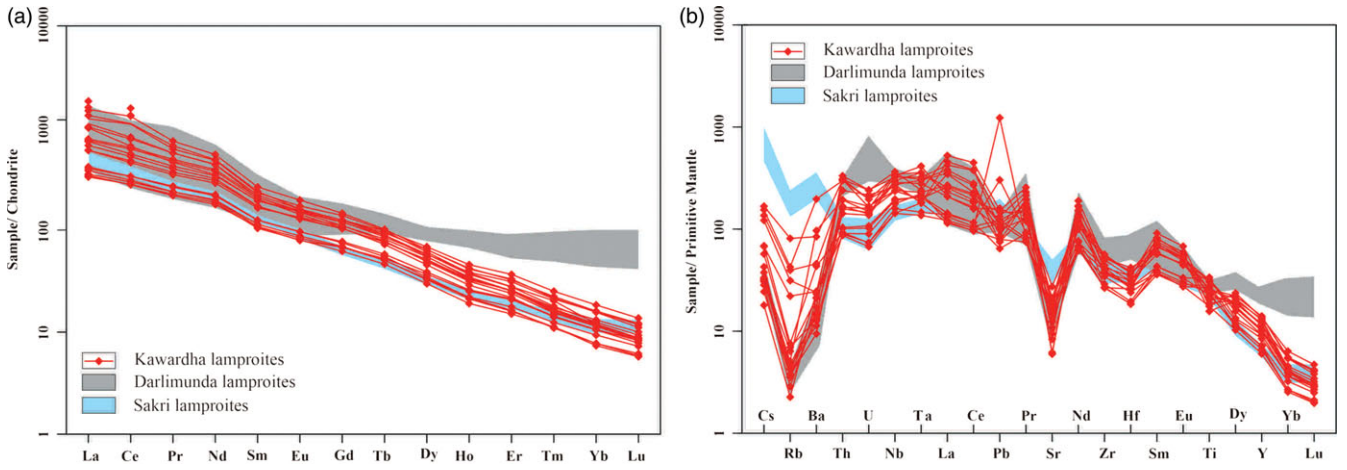

Figure 8. (a) Chondrite normalized rare earth element, and (b) primitive mantle normalized spider diagrams for Kawardha lamproites. Normalizing values of the Chondrite and primitive mantle are from Sun & McDonough (1989). Sakri lamproites (Chalapathi Rao *et al.* 2015) and Darlimunda lamproites are shown for comparison (Sahu *et al.* 2013; Santosh *et al.* 2018).

Post-magmatic alterations are more commonly accountable for the compositional modification of potassic-ultrapotassic rocks (Altherr *et al.* 2004; Mirnejad & Bell, 2006; Davies *et al.* 2006; Tappe *et al.* 2008). Elevated CaO (up to 22.3 wt%) and LOI values (up to 17.1 wt%; see Supplementary Table S1) in our samples indicate the formation of secondary carbonates and other hydrous minerals (e.g., calcite, dolomites and chlorites) through alteration. The Kawardha lamproites also exhibit low and/or highly variable contents of mobile elements like K (< 0.7wt%), Rb (1.4–51 ppm), Sr (126–577 ppm) and Ba (100–1400 ppm), suggesting alteration of samples. Alteration of olivine can be inferred from the lack of good correlation between MgO and Ni (Fig. 9a). Whereas a good correlation between immobile trace elements such as Hf vs. Zr (Fig. 9b), U vs. Th (Fig. 9c), Nb vs. Ta (Fig. 9d), and Cr vs. V (Fig. 9e) suggests that the concentration of immobile trace elements is appreciably not influenced by alteration processes and can be used to evaluate the petrogenetic processes.

5.c. Correlations with other lamproites of Bastar craton

The porphyritic texture, liquidus mineralogy (pseudomorphic olivine grains, Ti-phlogopites, prominent ulvospinel trend and abundance of apatite) and distinctive whole-rock chemistry (extremely silica undersaturated, enrichment of incompatible trace elements and REE fractionation patterns) are the chief characteristics of Kawardha lamproites. Regardless of modification in their whole-rock compositions, the mineral chemistry of phlogopite and spinel (Figs. 6, 7) and the overall trace element patterns (chondrite and primitive mantle normalized diagrams; Fig. 8) indicate the Kawardha lamproites are comparable to other lamproite occurrences of Bastar craton such as Sakri and Darlimunda lamproites (Sahu *et al.* 2013; Chalapathi Rao *et al.* 2015; Santosh *et al.* 2018). Moreover, similar trace element variations can be observed in Krishna lamproites (Reddy *et al.* 2003; Chalapathi Rao *et al.* 2010) of Dharwar craton and West Kimberly lamproites (Jaques, Lewis & Smith, 1986; Mitchell & Bergman, 1991).

Compared with other lamproite occurrences of the Bastar craton, the Kawardha lamproites are broadly similar to the Sakri lamproites (Figs. 6–8). The lamproites in the Darlimunda, Kalmidadar, Amlidadar and Parkom areas of the Nuapada field (Sahu *et al.* 2013; Chalapathi Rao *et al.* 2015; Santosh *et al.* 2018) exhibit relatively higher silica contents. Furthermore, the mica mineral chemistry of Darlimunda, Kalmidadar, Amlidadar and Parkom lamproites (Fig. 6) is closely related to West Kimberly lamproites, whereas the Sakri and Kawardha lamproites have geochemical similarities with the Krishna lamproites from the Eastern Dharwar craton in southern India (Chalapathi Rao *et al.* 2010). Micas from the Kawardha lamproites have lower Ti values (0.25–0.5 apfu; supplementary Table S3) than those of other lamproites reported from the Bastar craton (Ti = 0.5–0.9 apfu; Fig. 6b, c). Based on the mica composition and whole-rock elemental variations, Kawardha lamproites exhibit distinct similarities with Sakri lamproites. However, Kawardha lamproite samples have high LREEs (400–1100 times of chondrites) in contrast to Sakri lamproites (LREEs = 400–500 times of chondrites). Whereas, Darlimunda lamproites (Santosh *et al.* 2018) have appreciably higher HREE (10–40 times of chondrites) contents as compared to Kawardha lamproites (10–20 times of chondrites) and Sakri lamproites (20–30 times of chondrites). The concentrations of LREEs and HREEs in the Bastar lamproites suggest an enriched mantle source. Nevertheless, the LREE contents and $(La/Yb)_N$ ratio of the Kawardha lamproites are higher than that of Sakri lamproite but have considerably similar contents of HREEs (Fig. 8). However, Darlimunda lamproites have slightly higher HREEs compared to Kawardha and Sakri lamproites. The initial bulk rock Sr (0.705865–0.709024) and Nd (0.511063–0.511154) isotopic ratios of Sakri lamproites also point out the enriched source (Chalapathi Rao *et al.* 2015).

Previously, Lakra & Kujur (2021) suggested both orogenic and anorogenic origins for the Kawardha lamproites. However, the data of Lakra & Kujur (2021) show low REEs (REE = 59–98 ppm) in the lamproite samples, which are not consistent with other lamproite occurrences. Our new analysis from the Kawardha lamproites shows significantly higher REEs (REE = 406–1596 ppm), which can be correlated with other lamproite occurrences in the Bastar craton. The studied samples (Supplementary Table S9) contain normative olivine (up to 28%), cpx (up to 38%) and leucite (< 1%), which suggests a close affinity towards olivine lamproites rather than leucite lamproites.

In summary, our geochemical comparison of lamproite occurrences in the Bastar craton reveals that Kawardha lamproites share significant geochemical similarities with the Sakri lamproites and other lamproites of the Bastar craton. This suggests, despite the differences in emplacement ages, a common petrogenetic and tectonic process can be inferred for the Precambrian lamproites of Bastar craton.

https://doi.org/10.1017/S0016756825100186 Published online by Cambridge University Press

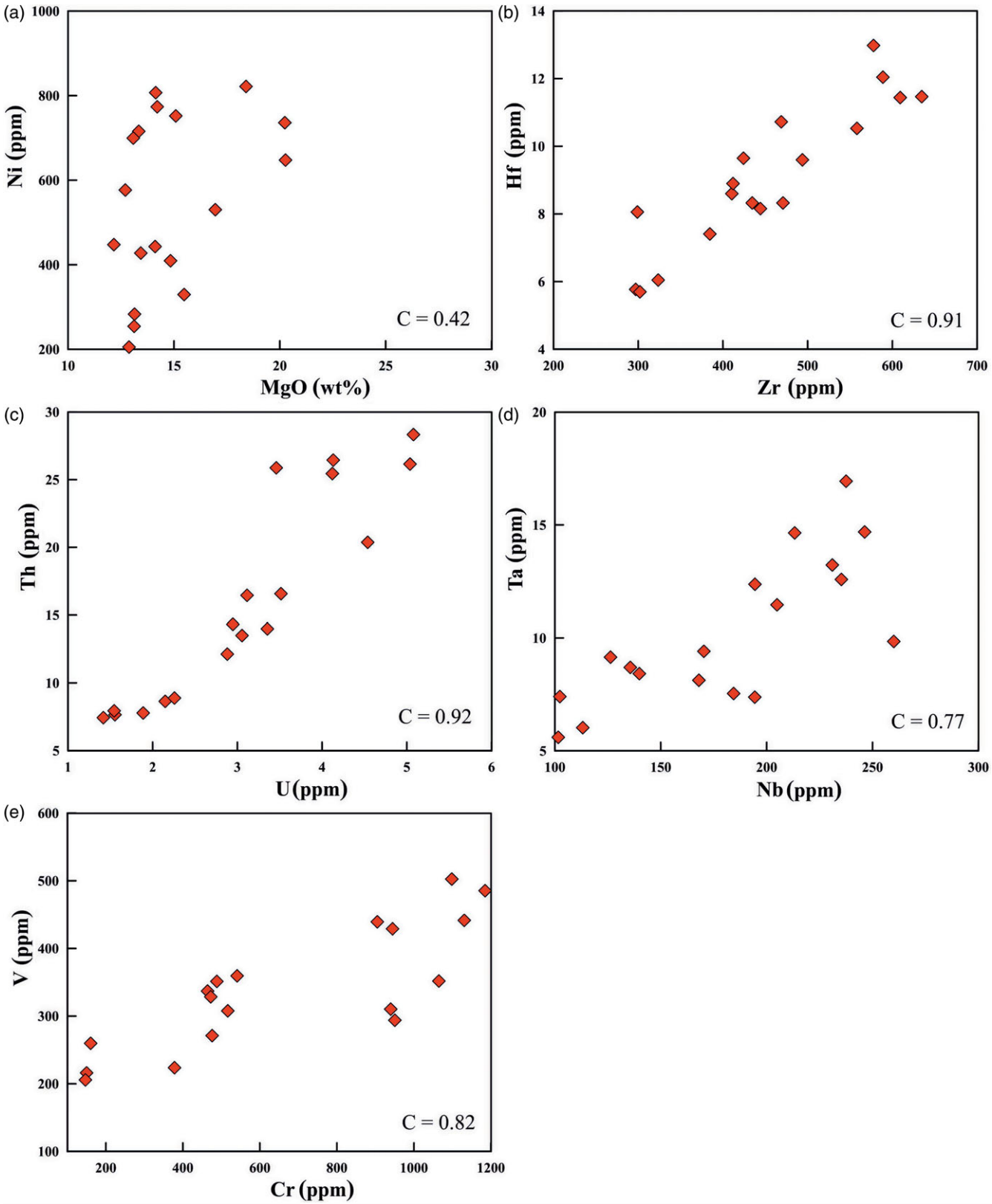

Figure 9. Bivariate plots involving major elements (wt%) and trace elements (ppm) of the Kawardha lamproites: (a) MgO wt% vs. Ni, (b) Zr vs. Hf, (c) U vs. Th, (d) Nb vs. Ta, (e) Cr vs. V.

https://doi.org/10.1017/S0016756825100186 Published online by Cambridge University Press

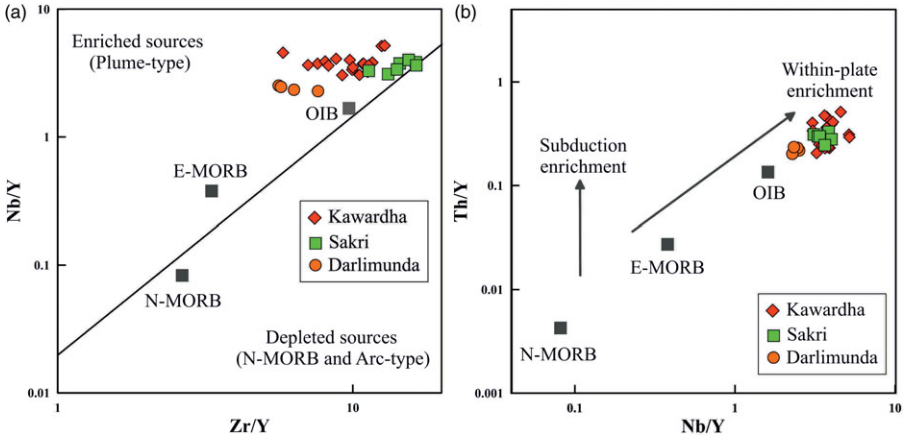

Figure 10. Relative HFSE abundance in the Kawardha lamproite samples, (a) Nb/Y vs. Zr/Y plot (after Fitton *et al.* 1997). (b) Th/Y vs. Nb/Y plot interpreted as evidence for within-plate enrichment. Average N-MORB, E-MORB and OIB compositions from Sun & McDonough (1989). Darlimunda (Santosh *et al.* 2018) and Sakri (Chalapathi Rao *et al.* 2015) are also plotted for comparison.

5.d. Melting conditions of a heterogeneous mantle source and petrogenesis of Kawardha lamproites

The primitive mantle normalized multi-element diagram (Fig. 8a) of Kawardha lamproites exhibits negative anomalies of Rb, Sr and Zr, which indicates the fractionation of various phases. The Rb in multi-element plot signifies residual amphibole or phlogopite (Sato, Katsura & Ito, 1997), Sr marks the fractionation of clinopyroxenes (Tappe *et al.* 2004) and Zr accounts for zirconium silicate in the residuum (Mitchell & Edgar, 2002). The primitive mantle signatures (positive Nb, Ta and Ti anomaly) of the Kawardha lamproite rule out the subduction-related origin.

The high MgO, compatible (Ni, Co, Cr) and incompatible (Ba, Zr, Hf, Nb, LREEs) trace element concentrations and low Al_2O_3 are comparable to other anorogenic lamproites worldwide (Jaques Lewis & Smith, 1986; Mitchell & Bergman, 1991; Sahu *et al.* 2013; Chalapathi Rao *et al.* 2010, 2015; Santosh *et al.* 2018). Enrichment of LREE over HREE, high La/Yb (50–159) and Dy/Yb (5.1–7.6) ratios, together with a high concentration of compatible trace elements (such as Ni, Cr, Co), suggests the presence of a garnet-bearing source (Mitchell & Bergman, 1991; Mirnejad & Bell, 2006; Davidson *et al.* 2013). The ratios of highly and moderately incompatible trace elements (average La/Nb = 0.93 and average Sm/Yb = 13.34) indicate low-degree partial melting of the mantle peridotite sources within the garnet stability field and mixing of heterogeneous melts. (Stracke & Bourdon, 2009). Kawardha lamproites exhibit high values of Zr/Hf ratio (37.35–55.17) along with enrichment in LREE, which suggests low degree partial melting of the mantle source (Fraser *et al.* 1985; Foley, 1992; Hart & Dunn, 1993; Tainton & McKenzie, 1994; Weyer *et al.* 2003). Similar enrichment of incompatible and compatible trace elements in the melt often involves cryptic and/or modal metasomatism and the development of metasomatic veins (Foley, 1992). The dehydration reactions or partial melting of the subducted crust also induce metasomatic reactions in the lithospheric mantle. Low-degree partial melting of this heterogeneous mantle source can lead to the formation of lamproite magma (Davies *et al.* 2006; Prelevic, Foley & Cvetkovic, 2007; Akal 2008). The positive anomalies of Nb-Ta on the primitive mantle normalized plot (Fig. 8b) together with Zr/Y, Th/Y and Nb/Y ratios (Fig. 11a, b) suggest that asthenospheric mantle was involved in their genesis (Tainton & McKenzie, 1994; Choukroun *et al.* 2005; Mirnejad & Bell 2006). Earlier researchers (Mitchell & Bergman, 1991; Miller *et al.* 1999) postulated that the lamproite magma originates from the low degree of partial melting of the phlogopite-bearing metasomatized mantle source. Partial melting of phlogopite-bearing mantle source

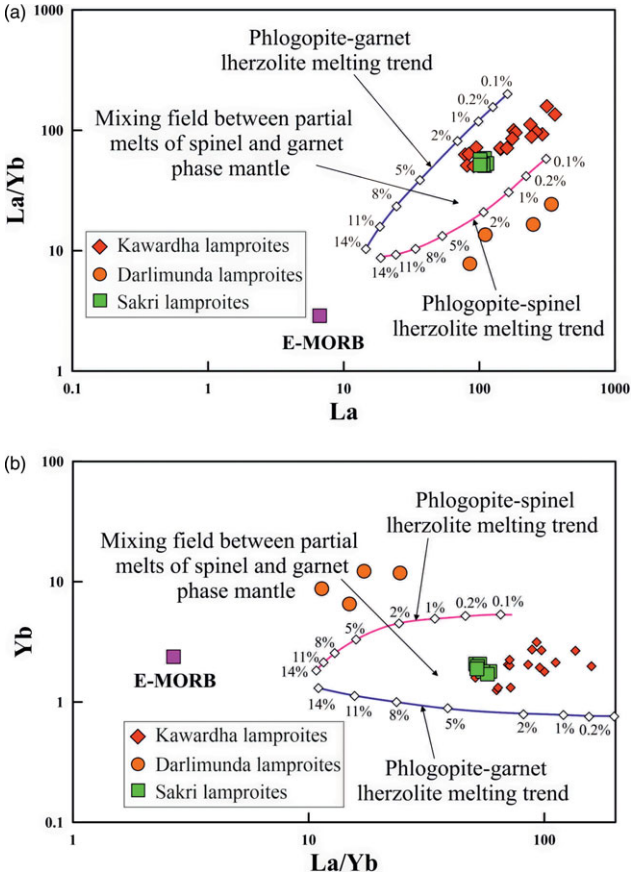

Figure 11. Trace element ratios of the Kawardha lamproite samples (a) La vs. La/Yb, and (b) La/Yb vs. Yb. Non-modal batch melting curves for phlogopite-bearing spinel and garnet lherzolites. Phlogopite-spinel and phlogopite-garnet lherzolites are from Miller *et al.* (1999). The sources are (i) phlogopite–spinel lherzolite: 0·55 ol, 0·25 opx, 0·11 cpx, 0·03 sp, 0·08 phl; and (ii) phlogopite–garnet lherzolite: 0·55 ol, 0·19 opx, 0·07 cpx, 0·11 gt, 0·08 phl. E-MORB (after Sun & McDonough, 1989), Darlimunda (Santosh *et al.* 2018) and Sakri (Chalapathi Rao *et al.* 2015) are also plotted for comparison.

can be accomplished by peritectic melting under the water-saturated condition (Foley, 1993). The non-modal partial melting curves for phlogopite-bearing spinel and garnet lherzolites were generated to estimate the degree of partial melting. The composition of phlogopite-spinel and phlogopite-garnet lherzolite sources is from Miller *et al.* (1999). The La vs. La/Yb (Fig. 11a) and La/Yb vs. Yb (Fig. 11b) exhibit that the Kawardha lamproites can be formed by the small degree of partial melting (0.1–2%) of the

https://doi.org/10.1017/S0016756825100186 Published online by Cambridge University Press

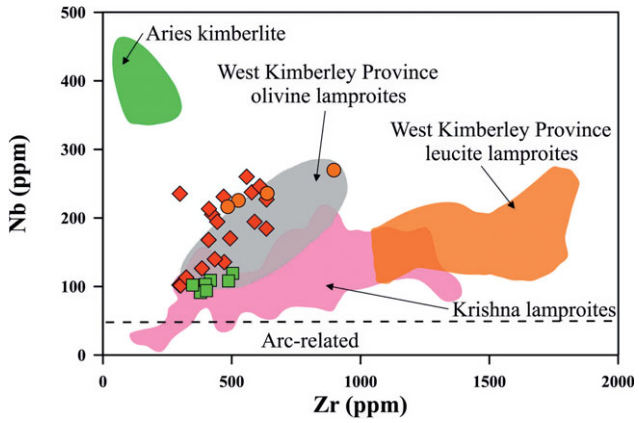

Figure 12. Zr vs. Nb diagram depicting the arc and non-arc setting. The dotted line represents the field of rocks with very low Nb (< 50 ppm), which are considered to be subduction-related tectonic settings (Sheppard & Taylor, 1992). The field of Krishna lamproites (Paul *et al.* 2007; Chalapathi Rao *et al.* 2010), West Kimberly province olivine lamproites, West Kimberly province leucite lamproites and Aries kimberlites (Foley *et al.* 1987; Altherr *et al.* 2004) is shown for comparison. Darlimunda (Santosh *et al.* 2018) and Sakri (Chalapathi Rao *et al.* 2015) are also plotted for comparison.

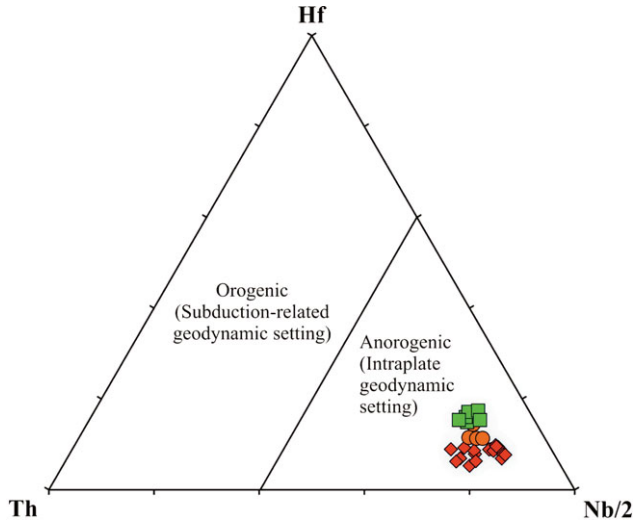

Figure 13. Hf vs. Th vs. Nb/2 ternary tectonic discrimination diagram (after Krmíček *et al.* 2011) representing anorogenic geodynamic setting for the Kawardha lamproites. Darlimunda and Sakri lamproites are plotted for comparison. Sakri lamproites (Chalapathi Rao *et al.* 2015) and Darlimunda lamproites (Sahu *et al.* 2013; Santosh *et al.* 2018) are shown for comparison.

phlogopite-bearing lherzolite in which melt contribution is from both garnet and spinel stability fields.

5.e. Tectonic setting of Kawardha lamproites

The high field strength elements (HFSEs) such as Zr and Nb are widely used to distinguish between intra-cratonic ultrapotassic alkaline rocks and other arc-related rocks because of their immobile behaviour during various low-grade post-magmatic alterations (Paton *et al.* 2009). In the Zr vs. Nb diagram (Fig. 12), the Kawardha lamproites do not show any arc signatures. An

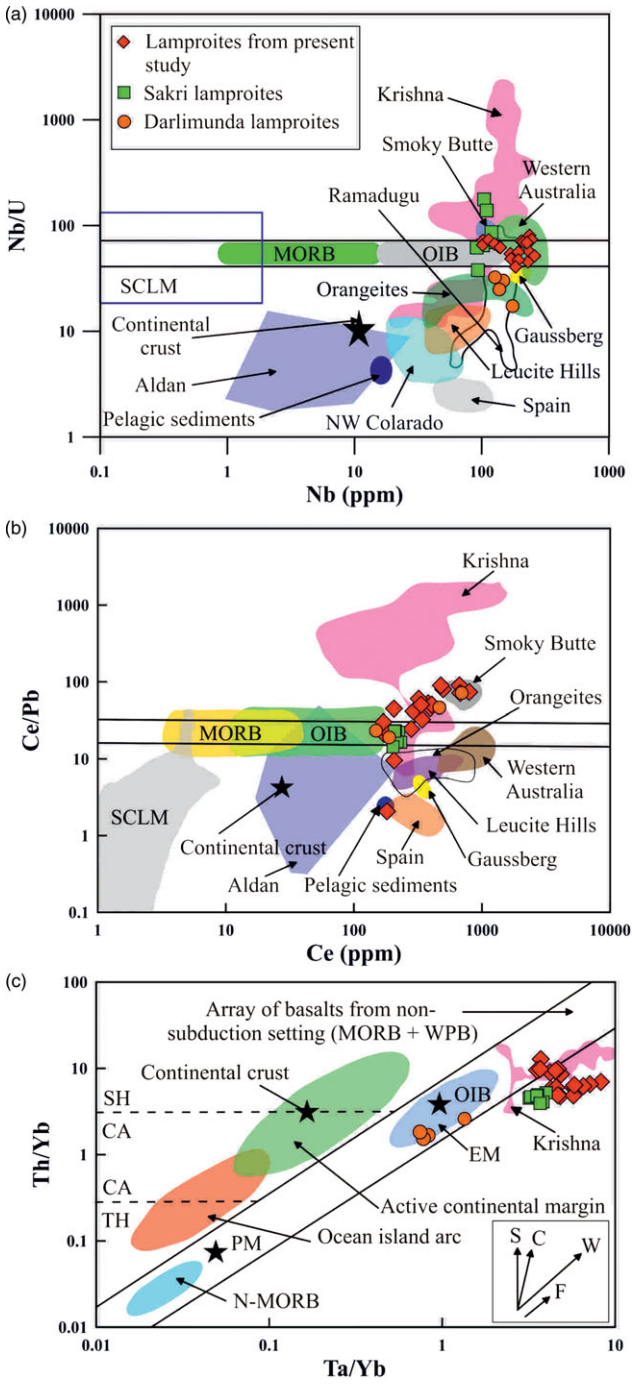

Figure 14. (a) Nb/U vs. Nb, (b) Ce/Pb vs. Ce and (c) Ta/Yb vs. Th/Yb plots for the Kawardha lamproites. The mantle array includes constructive plate boundary magmas (normal midocean ridge basalts: N-MORB; enriched midocean ridge basalts; E-MORB) and within-plate alkaline basalts (ocean island basalts; OIB). AUCC: Archean upper continental crust. SCLM: sub-continental lithospheric mantle. Fields for convergent margin basalts include the tholeiitic (TH), calc-alkaline (CA) and shoshonitic (SHO) magma series. The vectors S, C, W and f refer to subduction zone components, crustal contamination, within-plate fractionation and fractional crystallization, respectively (after Pearce, 2008). Fore arc, arc and back-arc fields of recent convergent margins are from Metcalf and Shervais (2008). Various fields of lamproites are taken from Davies *et al.* (2006), Yilmaz (2010), Paul *et al.* (2007) and Chalapathi Rao *et al.* (2010). Plots of Sakri lamproites (Chalapathi Rao *et al.* 2015) and Darlimunda lamproites (Sahu *et al.* 2013; Santosh *et al.* 2018) are also shown for comparison. Data symbols are the same as in Figure 6.

https://doi.org/10.1017/S0016756825100186 Published online by Cambridge University Press

anorogenic tectonic setting can also be inferred from the Th-Hf-Zr/2 diagram (Fig. 13).

In the Nb/U vs. Nb (Fig. 14a), Ce/Pb vs. Ce (Fig. 14b) and Ta/Yb vs. Nb/Y (Fig. 14c) plots, the lamproite samples from the present study fall very close to oceanic island basalts (OIB) within the mantle array, which implies a deep mantle source for the primary magma (Santosh *et al.* 2018). However, to evaluate the degree of enrichment or depletion of mantle source, Zr/Y vs. Nb/Y (Fig. 10a; after Fitton *et al.* 1997) and Th/Y vs. Nb/Y (Fig. 10b; after Sun & McDonough, 1989) ratios were employed in the present study. The high values of Zr/Y (5.8–12.8), Nb/Y (3–5.2), Th/Y (0.2–0.5), Nb/Yb (71–110) and Ta/Yb (3.5–8.3) ratios suggest enriched or fertile mantle domains like OIBs.

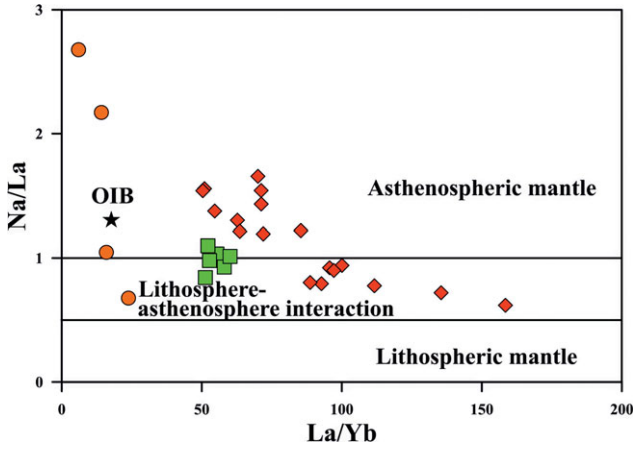

Figure 15. La/Yb vs. Nb/La diagram depicts an asthenosphere magma source and interaction of lithospheric and asthenospheric mantle components for the Kawardha lamproites and other lamproites from eastern Baster Craton (modified after Smith *et al.* 1999). Darlimunda (Santosh *et al.* 2018) and Sakri (Chalapathi Rao *et al.* 2015) are also plotted for comparison. The average OIB composition was taken from Fitton, James & Leeman (1991).

Lamproite and other ultrapotassic magmatism reported from several parts of the Bastar craton have been correlated with intra-continental rifting (Yellappa, Chalapathi Rao & Chetty, 2010; Lehmann *et al.* 2010; Sahu *et al.* 2013; Chalapathi Rao *et al.* 2015; Santosh *et al.* 2018). We noticed that most of the lamproitic samples of Kawardha, Darlimunda (Santosh *et al.* 2018) and Sakri (Chalapathi Rao *et al.* 2015) from Bastar craton plot in the asthenosphere and lithosphere-asthenosphere interaction array on La/Yb vs. Nb/La diagram (Fig. 15). This further points out that the melting might have initiated at the asthenospheric sources beneath Bastar craton and the melt possibly interacted with the metasomatized lithospheric mantle domains (Fig. 16). In the Bastar craton, active subduction and arc magmatism have been noticed from the Mesoarchean to the Neoarchean (Santosh *et al.* 2020, Manu Prasanth *et al.* 2018). The Paleoproterozoic granites and layered gabbro-anorthositic complexes in the central part of the craton are proposed to have formed in a post-collisional tectonic regime (Manu Prasanth *et al.* 2023). The recycling of early crustal domains might have significantly contributed to the metasomatism of the previously depleted SCLM. Santosh *et al.*

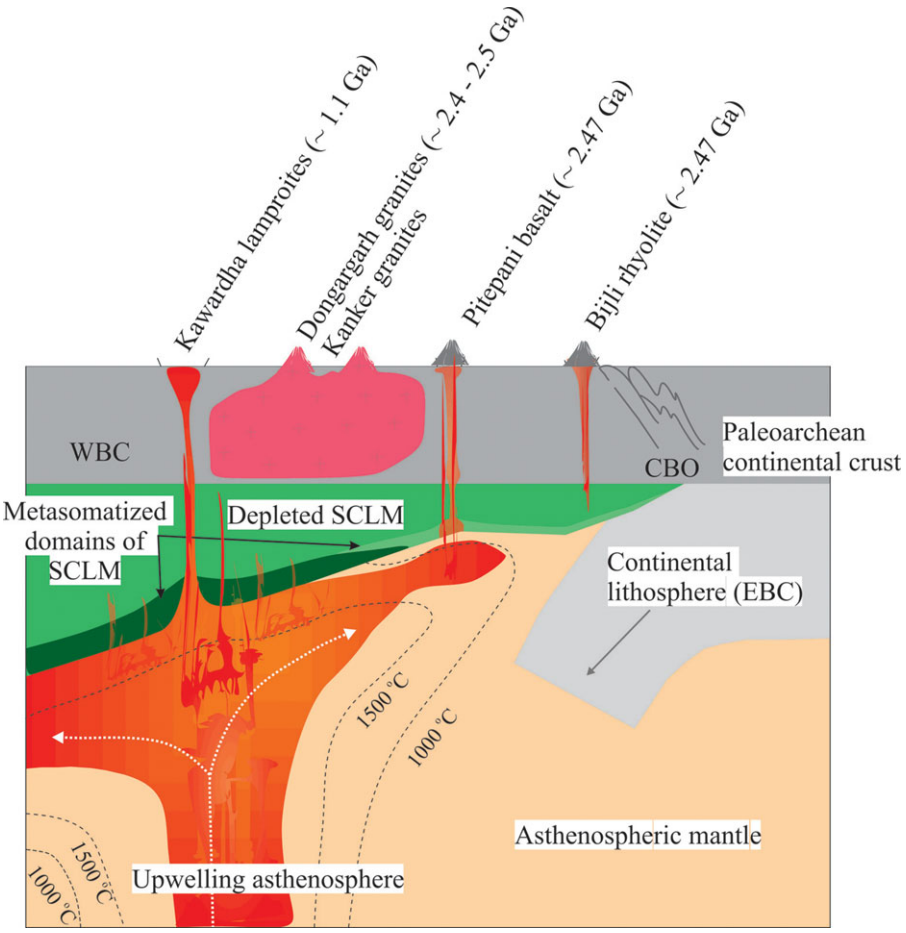

Figure 16. Schematic diagram showing the emplacement of Kawardha lamproites in the WBC. The possible formation conditions of Pitepani and Bijli volcanic rocks, Dongargarh and Kanker granitic intrusions of WBC are also shown.

https://doi.org/10.1017/S0016756825100186 Published online by Cambridge University Press

(2018) postulated that the melt source for the eastern Bastar lamproites (Sakri and Darlimunda) was derived from the asthenospheric mantle, and further interactions with the lithosphere caused variable enrichments in the source. Such enrichment in the deep mantle melts occurs due to assimilating the earlier formed metasomatic veins in the lithospheric mantle source (Pilet, Baker & Stolper, 2008; Pilet *et al.* 2011; Niu, 2008). The Kawardha lamproite magmatism is possibly related to the Archean subduction-related metasomatic modification of the SCLM along the eastern margin of the WBC. The interactions with the asthenospheric melts and metasomatized and phlogopite-rich SCLM domains further lead to the formation of the parental melts of Kawardha lamproites. The observed geochemical variations and comparisons with other lamproite occurrences in the EBC further imply that Kawardha lamproites were placed in an intra-cratonic rift setting in the Bastar craton.

6. Conclusions

1. The ultrabasic lamproite dykes from the Kawardha area are compositionally equivalent to olivine-phlogopite lamproites and are characterized by phenocrysts and microphenocrysts of pseudomorphic olivine, phlogopite, spinel within chlorite – and carbonate-rich groundmass together with rutile and apatite as accessory phases.
2. The Kawardha lamproite dykes are generated by low degree (up to 2%) partial melting of the mixed phlogopite-spinel and phlogopite-garnet lherzolite source. The melt possibly originated within the asthenospheric mantle; further asthenosphere-lithosphere interaction causes the enrichment of incompatible trace elements.
3. The subduction-related crustal recycling in the Archean and Paleoproterozoic Bastar craton has led to the metasomatic enrichment of the SCLM domains. The Mesoproterozoic rifting events in the craton caused the asthenospheric mantle melts to interact with the metasomatized domains of SCLM, which created the parental melts of the Kawardha lamproites.

Supplementary material. The supplementary material for this article can be found at https://doi.org/10.1017/S0016756825100186

Acknowledgements. The First author (TH) is thankful to NIT, Raipur, for providing all the necessary facilities and financial assistance (institute fellowship) to carry out the present research work. We are grateful to the XRF & HR-ICP-MS laboratory of NGRI, Hyderabad, and the EPMA laboratory of the Department of Earth Sciences, IIT Bombay, for providing the analytical facilities. Dayanand Tigga, Arth Rawal and Jayant Nayak are also acknowledged for their effortless assistance during fieldwork.

Competing interests. The authors declare no conflict of interest.

References

Akal C (2008) K-richterite-olivine-phlogopite-diopside-sanidine lamproites from the Afyon volcanic province, Turkey. *Geological Magazine* **145**, 570–85.

Altherr R, Meyer HP, Holl A, Volker F, Alibert C and McCulloch MV (2004) Geochemical and Sr-Nd-Pb isotopic characteristics of late Cenozoic leucite lamproites from the east European Alpine Belt (Macedonia and Yugoslavia). *Contributions to Mineralogy and Petrology* **147**, 58–73.

Avanzinelli R, Lustrino M, Mattei M, Melluso L and Conticelli S (2009) Potassic and ultrapotassic magmatism in the circum-Tyrrhenian region: significance of carbonated pelitic vs. pelitic sediment recycling at destructive plate margins. *Lithos* **113**, 213–27.

Bergman SC (1987) Lamproites and other potassium-rich igneous rocks: a review of their occurrence, mineralogy and geochemistry. *Geological Society, London, Special Publications* **30**, 103–90.

Chalapathi Rao NV, Kamde G, Kale HG and Dongre A (2010) Mesoproterozoic lamproites from the Krishna Valley, Eastern Dharwar Craton, southern India: petrogenesis and diamond prospectivity. *Precambrian Research* **177**, 103–30.

Chalapathi Rao NV, Burgess R, Nanda P, Choudhary AK, Sahoo S, Lehmann B and Chahong N (2015) Petrology, 40Ar/39Ar age, Sr-Nd isotope systematics, and geodynamic significance of an ultrapotassic (lamproitic) dyke with affinities to kamafugite from the easternmost margin of the Bastar Craton, India. *Mineralogy and Petrology* **110**, 269–93.

Choukroun M, O'Reilly SY, Griffin WL, Pearson NJ and Dawson JB (2005) Hf isotopes of MARID (mica-amphibole-rutile-ilmenite-diopside) rutile trace metasomatic processes in the lithospheric mantle. *Geology* **33**, 45–8.

Davidson J, Turner S and Plank T (2013) Dy/Dy* variations arising from mantle sources and petrogenetic processes. *Journal of Petrology* **54**, 525–37.

Davies GR, Stolz AJ, Mahotkin IL, Nowell GM and Pearson DG (2006) Trace element and Sr–Pb–Nd–Hf isotope evidence for ancient, fluid-dominated enrichment of the source of Aldan Shield lamproites. *Journal of Petrology* **47**, 1119–46.

DePaolo DJ (1981) Trace element and isotopic effects of combined wall rock assimilation and fractional crystallization. *Earth and Planetary Science Letters* **53**, 189–202.

Deshmukh SD, Hari KR, Diwan P and Prasanth MM (2018) Geochemical constraints on the tectonic setting of the Sonakhan greenstone belt, Bastar Craton, Central India. *Acta Geochimica* **37**, 489–99.

Dostal J and Dupuy C (1984) Geochemistry of the North Mountain basalts (Nova Scotia, Canada). *Chemical Geology* **45**, 245–61.

Edgar AD and Charbonneau HE (1991) Fluorine-bearing phases in lamproites. *Mineralogy and Petrology* **44**, 125–49.

Edgar AD, Pizzolato LA and Sheen J (1996) Fluorine in igneous rocks and minerals with emphasis on ultrapotassic mafic and ultramafic magmas and their mantle source regions. *Mineralogical Magazine* **60**, 243–57.

Ezad IS and Foley SF (2022) Experimental partitioning of fluorine and barium in lamproites. *American Mineralogist* **107**, 2008–19.

Fipke CE, Gurney JJ and Moore RO (1995) *Diamond Exploration Techniques Emphasizing Indicator Mineral Geochemistry and Canadian Examples*. Ottawa, Canada: Geological Survey of Canada Bulletin.

Fitton JG, James D and Leeman WP (1991) Basic magmatism associated with late Cenozoic extension in the western United States: compositional variations in space and time. *Journal of Geophysical Research - Solid Earth* **96**, 13693–711.

Fitton JG, Saunders AD, Norry MJ, Hardarson BS and Taylor RN (1997) Thermal and chemical structure of the Iceland plume. *Earth and Planetary Science Letters* **153**, 197–208.

Foley S (1992) Petrological characterization of the source components of potassic magmas: geochemical and experimental constraints. *Lithos* **28**, 187–204.

Foley SF (1993) An experimental study of olivine lamproite: first results from the diamond stability field. *Geochimica et Cosmochimica Acta* **57**, 483–89.

Foley S, Venturelli G, Green DH and Toscani L (1987) The ultrapotassic rocks: characteristics, classification, and constraints for petrogenetic models. *Earth Science Reviews* **24**, 81–134.

Förster MW, Buhre S, Xu B, Prelević D, Mertz-Kraus R and Foley SF (2019a) Two-stage origin of K-enrichment in ultrapotassic magmatism simulated by melting of experimentally metasomatized mantle. *Minerals* **10**, 41.

Förster MW, Prelević D, Buhre S, Mertz-Kraus R and Foley SF (2019b) An experimental study of the role of partial melts of sediments versus mantle melts in the sources of potassic magmatism. *Journal of Asian Earth Sciences* **177**, 76–88.

Fraser KJ, Hawkesworth CJ, Erlank AJ, Mitchell RH and Scott-Smith BH (1985) Sr, Nd and Pb isotope and minor element geochemistry of lamproites and kimberlites. *Earth and Planetary Science Letters* **76**, 57–70.

Ghosh JG (2004) 3.56 Ga tonalite in the central part of the Bastar Craton, India: oldest Indian date. *Journal of Asian Earth Sciences* **23**, 359–64.

Gibson SA, Thompson RN, Dickin AP and Leonardos OH (1995) High-Ti and low-Ti mafic potassic magmas: key to plume-lithosphere interactions

and continental flood-basalt genesis. *Earth and Planetary Science Letters* **136**, 149–65.

Gülmez F, Prelević D, Förster MW, Buhre S and Günther J (2023) Experimental production of K-rich metasomes through sediment recycling at the slab-mantle interface in the fore-arc. *Scientific Reports* **13**, 19608.

Hart SR and Dunn T (1993) Experimental cpx/melt partitioning of 24 trace elements. *Contributions to Mineralogy and Petrology* **113**, 1–8.

Hofmann AW, Jochum KP, Seufert M and White WM (1986) Nb and Pb in oceanic basalts: new constraints on mantle evolution. *Earth and Planetary Science Letters* **79**, 33–45.

Huang XL, Niu Y, Xu Y, Chen LL and Yang QJ (2010) Mineralogical and geochemical constraints on the petrogenesis of post-collisional potassic and ultrapotassic rocks from Western Yunnan, SW China. *Journal of Petrology* **51**, 1617–54.

Jaques AL, Lewis JD and Smith CB (1986) *The Kimberlites and Lamproites of Western Australia*. Perth, Australia: Geological Survey of Western Australia Bulletin.

Kjarsgaard BA, Pearson DG, Tappe S, Nowell GM and Dowall DP (2009) Geochemistry of hypabyssal kimberlites from Lac de Gras, Canada: comparisons to a global database and applications to the parent magma problem. *Lithos* **112**, 236–48.

Krishna AK, Khanna TC and Mohan KR (2016) Rapid quantitative determination of major and trace elements in silicate rocks and soils employing fused glass discs using wavelength dispersive X-ray fluorescence spectrometry. *Spectrochimica Acta Part B: Atomic Spectroscopy* **122**, 165–71.

Krmíček L, Cempírek J, Havlín A, Príchystal A, Houzar S, Krmíčeková M and Gadas P (2011) Mineralogy and petrogenesis of a Ba–Ti–Zr-rich peralkaline dyke from Šebkovice (Czech Republic): recognition of the most lamproitic Variscan intrusion. *Lithos* **121**, 74–86.

Lakra A and Kujur SM (2021) Petrogenesis of Mesoproterozoic lamproite from Kawardha, Western Bastar Craton, Central India: insights from mineral, bulk rock and in-situ trace element geochemistry. *Indian Journal of Geosciences* **75**, 251–69.

Lehmann B, Burgess R, Frei D, Mainkar D, Chalapathi Rao NV and Heaman LM (2010) Diamondiferous kimberlites in central India synchronous with the Deccan flood basalts. *Earth and Planetary Science Letters* **290**, 142–49.

Liu D, Zhao Z, Zhu DC, Niu Y, DePaolo DJ, Harrison TM, Mo X, Dong G, Zhou S, Sun C, Zhang Z and Liu J (2014) Post collisional potassic and ultrapotassic rocks in southern Tibet: mantle and crustal origins in response to India–Asia collision and convergence. *Geochimica et Cosmochimica Acta* **143**, 207–31.

Manikyamba C, Santosh M, Chandan Kumar B, Rambabu S, Tang L, Saha A, Khelen AC, Ganguly S, Singh TD and Subba Rao DV (2016) Zircon U-Pb geochronology, Lu-Hf isotope systematics, and geochemistry of bimodal volcanic rocks and associated granitoids from Kotri Belt, Central India: implications for Neoarchean–Paleoproterozoic crustal growth. *Gondwana Research* **38**, 313–33.

Manu Prasanth MP, Hari KR, Chalapathi Rao NV, Hou G and Pandit D (2018) An island-arc tectonic setting for the Neoarchean Sonakhan Greenstone Belt, Bastar Craton, Central India: insights from the chromite mineral chemistry and geochemistry of the siliceous high-Mg basalts (SHMB). *Geological Journal* **53**, 1526–42.

Manu Prasanth MP, Hari KR, Chalapathi Rao NV, Santosh M, Hou G, Tsunogae T and Pandit D (2019) Neoarchean suprasubduction zone magmatism in the Sonakhan greenstone belt, Bastar Craton, India: implications for subduction initiation and melt extraction. *Geological Journal* **54**, 3980–4000.

Manu Prasanth MP, Sharma ASP, Santosh M, Yang CX and Hari KR (2023) Insights into the petrogenetic evolution of the Khallari layered intrusion and coeval granites of the Paleoproterozoic Dongargarh Supergroup, Bastar Craton, India. *Precambrian Research* **391**, 107040.

Martinotti G, Andreoli S, Giametta E, Poli V, Bria P and Janiri L (2006) The dimensional assessment of personality in pathologic and social gamblers: the role of novelty seeking and self-transcendence. *Comprehensive Psychiatry* **47**, 350–56.

Matchan E, Hergt J, Phillips D and Shee S (2009) The geochemistry, petrogenesis and age of an unusual alkaline intrusion in the western Pilbara Craton, Western Australia. *Lithos* **112**, 419–28.

McKenzie D (1989) Some remarks on the movement of small melt fractions in the mantle. *Earth and Planetary Science Letters* **95**, 53–72.

Meert JG, Pandit MK, Pradhan VR, Banks J, Sirianni R, Stroud M and Gifford J (2010) Precambrian crustal evolution of Peninsular India: a 3.0-billion-year odyssey. *Journal of Asian Earth Sciences* **39**, 483–515.

Metcalf RV and Shervais JW (2008) Suprasubduction-zone ophiolites: is there really an ophiolite conundrum? *Geological Society of America Special Papers* **438**, 191–222.

Miller C, Schuster R, Klötzli U, Frank W and Purtscheller F (1999) Post-collisional potassic and ultrapotassic magmatism in SW Tibet: geochemical and Sr–Nd–Pb–O isotopic constraints for mantle source characteristics and petrogenesis. *Journal of Petrology* **40**, 1399–424.

Mirnejad H and Bell K (2006) Origin and source evolution of the Leucite Hills lamproites: evidence from Sr–Nd–Pb–O isotopic compositions. *Journal of Petrology* **47**, 2463–89.

Mishra PK and Mohanty SP (2021) Geochemistry of carbonate rocks of the Chilpi Group, Bastar Craton, India: implications on ocean paleoredox conditions at the late Paleoproterozoic Era. *Precambrian Research* **353**, 106023.

Mitchell RH and Edgar AD (2002) Melting experiments on SiO2-rich lamproites to 6.4 GPa and their bearing on the sources of lamproite magmas. *Mineralogy and Petrology* **74**, 115–28.

Mitchell RH (1995) *Kimberlites, Orangeites and Related Rocks*. New York, USA: Plenum Press.

Mitchell RH and Bergman SC (1991) *Petrology of Lamproites*. New York, USA: Springer Science and Business Media.

Mohanty S (2015) Precambrian continent assembly and dispersal events of South Indian and East Antarctic Shields. *International Geology Review* **57**, 1992–2027.

Mohanty SP (2021) The Bastar Craton of Central India: tectonostratigraphic evolution and implications in global correlations. *Earth Science Reviews* **221**, 103770.

Murphy DT, Collerson KD and Kamber BS (2002) Lamproites from Gaussberg, Antarctica: possible transition zone melts of Archaean subducted sediments. *Journal of Petrology* **43**, 981–1001.

Nelson DR (1992) Isotopic characteristics of potassic rocks: evidence for the involvement of subducted sediments in magma genesis. *Lithos* **28**, 403–20.

Niu YL (2008) The origin of alkaline lavas. *Science* **320**, 883–4.

Paton C, Hergt JM, Woodhead JD, Phillips D and Shee SR (2009) Identifying the asthenospheric component of kimberlite magmas from the Dharwar Craton, India. *Lithos* **112**, 296–310.

Paul DK, Crockett JH, Reddy TAK and Pant NC (2007) Petrology and geochemistry including Platinum Group element abundances of the Mesoproterozoic ultramafic (lamproite) rocks of Krishna district, southern India: implications for source rock characteristics and petrogenesis. *Geological Society of India* **69**, 577–96.

Pearce JA (2008) Geochemical fingerprinting of oceanic basalts with applications to ophiolite classification and the search for Archean oceanic crust. *Lithos* **100**, 14–48.

Pilet S, Baker MB and Stolper EM (2008) Metasomatized lithosphere and the origin of alkaline lavas. *Science* **320**, 916–19.

Pilet S, Baker MB, Müntener O and Stolper EM (2011) Monte Carlo simulations of metasomatic enrichment in the lithosphere and implications for the source of alkaline basalts. *Journal of Petrology* **52**, 1415–42.

Prelevic D, Foley SF and Cvetkovic V (2007) A review of petrogenesis of Mediterranean Tertiary lamproites: a perspective from the Serbian ultra-potassic province. In *Cenozoic Volcanism in the Mediterranean Area* (eds L Beccaluva, G Banchini & M Wilson), pp. 113–29. Boulder, CO, USA: Geological Society of America.

Prelević D, Stracke A, Foley SF, Romer RL and Conticelli S (2010) Hf isotope compositions of Mediterranean lamproites: mixing of melts from asthenosphere and crustally contaminated mantle lithosphere. *Lithos* **119**, 297–312.

Rajesh HM, Mukhopadhyay J, Beukes NJ, Gutzmer J, Belyanin GA and Armstrong RA (2009) Evidence for an early Archaean granite from Bastar Craton, India. *Journal of Geological Society of London* **166**, 193–96.

Rapp RP, Irifune T, Shimizu N, Nishiyama N, Norman MD and Inoue T (2008) Subduction recycling of continental sediments and the origin of geochemically enriched reservoirs in the deep mantle. *Earth and Planetary Science Letters* **271**, 14–23.

https://doi.org/10.1017/S0016756825100186 Published online by Cambridge University Press

Ratre K, De Waele B, Biswal TK and Sinha S (2010) SHRIMP geochronology for the 1450 Ma Lakhna dyke swarm: its implication for the presence of Eoarchaean crust in the Bastar Craton and 1450–517 Ma depositional age for Purana Basin (Khariar), Eastern Indian Peninsula. *Journal of Asian Earth Sciences* **39**, 565–77.

Reddy TAK, Sridhar M, Ravi S, Chakravarthi V and Neelakantam S (2003) Petrography and geochemistry of the Krishna Lamproite Field, Andhra Pradesh. *Journal of Geological Society of India* **61**, 131–46.

Rock NMS (1991) *Lamprophyres*. Glasgow and London, UK: Blackie.

Rudnick R and Gao S (2003) Composition of the continental crust. In *The Crust: Treatise on Geochemistry* (ed RL Rudnick), pp. 1–64. Oxford, UK: Elsevier.

Rukhlov AS, Blinova AI and Pawlowicz JG (2013) Geochemistry, mineralogy and petrology of the Eocene potassic magmatism from the Milk River area, southern Alberta, and Sweet Grass Hills, northern Montana. *Chemical Geology* **353**, 280–302.

Sahu N, Gupta T, Patel SC, Khuntia DBK, Behera D, Pande K and Das SK (2013) Petrology of lamproites from the Nuapada Lamproite Field, Bastar Craton, India. *Journal of the Geological Society of India* **1**, 137–65.

Santosh M, Hari KR, He XF, Han YS and Prasanth MM (2018) Oldest lamproites from Peninsular India track the onset of Paleoproterozoic plume-induced rifting and the birth of large igneous province. *Gondwana Research* **55**, 1–20.

Santosh M, Tsunogae T, Yang CX, Han YS, Hari KR, Prasanth MM and Uthup S (2020) The Bastar Craton, central India: a window to Archean–Paleoproterozoic crustal evolution. *Gondwana Research* **79**, 157–84.

Sarkar S, Giuliani A, Phillips D, Howarth GH, Ghosh S and Dalton H (2022) Sublithospheric melt input in cratonic lamproites. *Geology* **50**, 1296–300.

Sato K, Katsura T and Ito E (1997) Phase relations of natural phlogopite with and without enstatite up to 8 GPa: implication for mantle metasomatism. *Earth and Planetary Science Letters* **146**, 511–26.

Satyanarayanan M, Balaram V, Sawant SS, Subramanyam KSV, Krishna GV and Dasaram B (2018) Rapid determination of REEs, PGEs, and other trace elements in geological and environmental materials by high resolution inductively coupled plasma mass spectrometry. *Atomic Spectroscopy* **39**, 1–15.

Sheppard S and Taylor WR (1992) Barium- and LREE-rich, olivine-micalamprophyres with affinities to lamproites, Mt. Bundey, Northern Territory, Australia. *Lithos* **28**, 303–25.

Smith EI, Sanchez A, Walker JD and Wang K (1999) Geochemistry of mafic magmas in the Hurricane Volcanic Field, Utah: implications for small- and large-scale chemical variability of the lithospheric mantle. *The Journal of Geology* **107**, 433–48.

Stern RJ, Leybourne MI and Tsujimori T (2016) Kimberlites and the start of plate tectonics. *Geology* **44**, 799–802.

Stracke A and Bourdon B (2009) The importance of melt extraction for tracing mantle heterogeneity. *Geochimica et Cosmochimica Acta* **73**, 218–38.

Sun SS and McDonough WF (1989) Chemical and isotopic systematics of oceanic basalts: implications for mantle composition and processes. *Geological Society, London, Special Publications* **42**, 313–45.

Sushchevskaya NM, Migdisova NA, Antonov AV, Krymsky RS, Belyatsky BV, Kuzmin DV and Bychkova YV (2014) Geochemical features of the Quaternary lamproitic lavas of Gaussberg Volcano, East Antarctica: result of the impact of the Kerguelen plume. *Geochemistry International* **52**, 1030–48.

Tainton KM and McKenzie D (1994) The generation of kimberlites, lamproites and their source rocks. *Journal of Petrology* **35**, 787–817.

Talukdar D, Pandey A, Chalapathi Rao NV, Kumar A, Pandit D, Belyatsky B and Lehmann B (2018) Petrology and geochemistry of the Mesoproterozoic Vattikod lamproites, Eastern Dharwar Craton, southern India: evidence for multiple enrichment of sub-continental lithospheric mantle and links with amalgamation and break-up of the Columbia supercontinent. *Contributions to Mineralogy and Petrology* **173**, 1–27.

Tappe S, Foley SF, Kjarsgaard BA, Romer RL, Heaman LM, Stracke A and Jenner GA (2008) Between carbonatite and lamproite—diamondiferous Torngat ultramafic lamprophyres formed by carbonate-fluxed melting of cratonic MARID-type metasomes. *Geochimica et Cosmochimica Acta* **72**, 3258–86.

Tappe S, Jenner GA, Foley SF, Heaman L, Besserer D, Kjarsgaard BA and Ryan B (2004) Torngat ultramafic lamprophyres and their relation to the North Atlantic Alkaline Province. *Lithos* **76**, 491–518.

Thompson RN, Dickin AP, Gibson IL and Morrison MA (1982) Elemental fingerprints of isotopic contamination of Hebridean Palaeocene mantle-derived magmas by Archaean sial. *Contributions to Mineralogy and Petrology* **79**, 159–68.

Thompson RN, Leat PT, Morrison MA, Hendry GL and Gibson SA (1990) Strongly potassic mafic magmas from lithospheric mantle sources during continental extension and heating: evidence from Miocene minettes of northwest Colorado, U.S.A. *Earth and Planetary Science Letters* **98**, 139–53.

Tommasini S, Avanzinelli R and Conticelli S (2011) The Th/La and Sm/La conundrum of the Tethyan realm lamproites. *Earth and Planetary Science Letters* **301**, 469–78.

Turner SP, Peate DW, Hawkesworth CJ, Eggins SM and Crawford AJ (1999) Two mantle domains and the time scales of fluid transfer beneath the Vanuatu arc. *Geology* **27**, 963–66.

Wagner C and Velde D (1986) The mineralogy of K-richterite bearing lamproites. *American Mineralogist* **71**, 17–37.

Wang Y, Foley SF and Prelevic D (2017) Potassium-rich magmatism from a phlogopite-free source. *Geology* **45**, 467–70.

Weyer S, Münker C and Mezger K (2003) Nb/Ta, Zr/Hf and REE in the depleted mantle: implications for the differentiation history of the crust–mantle system. *Earth and Planetary Science Letters* **205**, 309–24.

Xu W, Xu X and Zeng G (2017) Crustal contamination versus an enriched mantle source for intracontinental mafic rocks: insights from early Paleozoic mafic rocks of the South China Block. *Lithos* **286**, 388–95.

Yellappa T, Chalapathi Rao NV and Chetty TRK (2010) Occurrence of lamproites at the northern margin of the Indravati basin. *Journal of Geological Society of India* **75**, 632–45.

Yilmaz K (2010) Origin of anorogenic lamproite-like potassic lavas from the Denizli region in Western Anatolia extensional province, Turkey. *Mineralogy and Petrology* **99**, 219–39.

https://doi.org/10.1017/S0016756825100186 Published online by Cambridge University Press